FINAL TECHNICAL REPORT:
Award Number G10AP00009
The mechanics of episodic tremor and slip and potential for ETS triggered earthquakes

March 15, 2012

Paul Segall
(650-723-7241, segall@stanford.edu)
Geophysics Department
Stanford University
Stanford, CA 94305-2215

Award Dates: 1/1/2010 – 12/31/2011

Abstract

We developed a physical model of slow slip events based on dilatant strengthening. Our hypothesis is that rate-state frictional weakening allows transient slip to nucleate. As the shear rate increases, pores dilate, and restricted pore fluid flow makes the fault zone increasingly undrained. This decreases pore pressure and so increases the frictional resistance to further slip. The faster the fault slips, the harder it is for fluid flow into the fault zone to keep up with dilatancy; thus the stabilizing effect increases with slip speed. However, if slip becomes fast enough, frictional heat is generated leading to thermal pressurization. In this study we explored the competition between dilatant strengthening and thermal pressurization weakening, by developing numerical methods that solve the coupled elasticity, friction, and fluid and heat transport equations. We find that at lower background effective normal stress ($\bar{\sigma}$), slow slip events occur spontaneously, whereas at higher $\bar{\sigma}$, slip is inertially limited. At intermediate $\bar{\sigma}$, dynamic events are followed by quiescent periods, and then long durations of repeating slow slip events. In these cases, accelerating slow events ultimately nucleate dynamic rupture.

We develop depth dependent numerical models meant to represent conditions appropriate for the Cascade subduction zone. We find that model slow slip events spontaneously nucleate in areas of low ambient effective normal stress and velocity weakening friction. We observe two classes of behavior. When the low effective stress velocity weakening (LESVE) region is large relative to a critical nucleation dimension SSE tend to propagate further up-dip with time. As the model SSE continue, the maximum slip speed generally increases, such that ultimately thermal pressurization becomes important and the fault accelerates to dynamic instability. If on the other hand the size of the LESVE region is sufficiently small, model SSE become trapped in this region. SSE transfer stress to the region up-dip of the ETS zone, eventually leading to the nucleation of a dynamic event just up-dip of the ETS zone. The possibility that an ETS event can evolve into a dynamic event should be considered when assessing seismic hazards in the Pacific Northwest.

One hypothesis for occurrence of tremor is that locked asperities within the SSE region are loaded by the surrounding slip, leading to localized dynamic rupture. This suggests that tremor is favored in areas of high slip-rate immediately behind the slow-slip front. To test this we inverted daily GPS positions for the space-time evolution of slip and slip-rate on the plate interface during the August 2009 ETS event, and compared the slip-rate to tremor epicenters independently determined from seismic data. We find that the tremor epicenters are indeed very well correlated with the areas of instantaneously high slip-rate, supporting the hypothesis.

1 Introduction

Dilatant strengthening has been proposed as a mechanism for slow slip events (SSE) [Segall et al., 2010, Suzuki and Yamashita, 2009, Liu and Rubin, 2010, Yamashita and Suzuki, 2011]. Dilatancy, the tendency for pore space to increase under shear, is intrinsic to compacted granular materials, including fault gouges. Rate-state frictional weakening allows transient slip to nucleate. As the shear rate increases, pores dilate, and restricted pore fluid flow makes the fault zone increasingly undrained. This decreases pore pressure p, increasing the effective normal stress $\bar{\sigma} \equiv (\sigma - p)$, and so increases the frictional resistance to further slip. The faster the fault slips, the harder it is for fluid flow into the fault zone to keep up with dilatancy; thus the stabilizing effect increases with slip speed. However, if slip becomes fast enough, frictional heat is generated faster than can be removed by conduction. The greater thermal expansivity

of water relative to rock leads to an *increase* in p and so a decrease in frictional resistance. Because the thermal expansivity is greater than that of rock, this leads to an *increase* in p, and a decrease in frictional resistance. In this study we explored the competition between dilatant strengthening and thermal pressurization weakening.

2 Governing Equations

We take the fault zone to lie in the plane $y = 0$, and take the limit that the shear zone thickness $h \to 0$. Deformation is assumed to be plane strain in the x, y plane (slip in the x-direction). We employ the radiation damping approximation of elastodynamics [Rice, 1993] such that the momentum balance on the fault is

$$\tau_0 + \frac{\mu}{2\pi(1-\nu)} \int_{-\infty}^{\infty} \frac{\partial\delta/\partial\xi}{\xi - x} d\xi - f(v,\theta)[\sigma - p(y=0)] = \frac{\mu}{2v_s} v. \tag{1}$$

The difference between the elastic stress and the frictional resistance is balanced by the stress change associated with plane shear waves (with velocity v_s) radiating from the fault. The first term on the left is the shear stress acting on the fault in the absence of slip, the second represents the elastic stress due to gradients in slip δ, and the third term is the frictional resistance. The friction coefficient is a function of sliding velocity v and state variable θ. For anti-plane geometry we simple replace $\mu/(1-\nu)$ with μ. This "quasi-dynamic" formulation leads to a reasonable representation of dynamic slip, although maximum slip speeds and propagation rates are inaccurate [Lapusta and Liu, 2009].

To investigate the role of dilatancy and thermal pressurization during fault slip, we consider coupled friction, dilatancy, heat, and pore fluid flow. Neglecting conduction parallel to the fault (the x-direction) and heat advection in the pore fluid phase [Lachenbruch, 1980], and assuming spatially uniform thermal properties, the heat equation in the limit $h \to 0$, reduces to a homogeneous diffusion equation, with the frictional heat production appearing as a boundary condition [Rice, 2006]:

$$\frac{\partial T}{\partial t} = c_{\text{th}} \frac{\partial^2 T}{\partial y^2}; \qquad \left.\frac{\partial T}{\partial y}\right|_{y=0} = -\frac{\tau v}{2c\rho c_{\text{th}}}. \tag{2}$$

For $c_{\text{th}} \sim 10^{-6}$ m^2/s, a thermal anomaly penetrates on the order of a few meters in the one year cycle time for typical slow slip events. Because this distance is much less than the tens of kilometer dimensions of SSE, gradients in the along-fault direction are likely to be extremely small relative to those in the across-fault direction. Therefore, we can neglect conduction parallel to the fault.

Neglecting pore fluid flow parallel to the fault for the same reason that heat flow in this direction is negligible, changes in pore pressure are given by

$$\frac{\partial p}{\partial t} = \frac{1}{\eta\beta} \frac{\partial}{\partial y}\left(\kappa \frac{\partial p}{\partial y}\right) + \Lambda \frac{\partial T}{\partial t} - \frac{1}{\beta}\frac{\partial \phi}{\partial t}, \tag{3}$$

where η is pore fluid viscosity, β is the compressibility of the fluid and the pore space, κ is the permeability, ϕ is the inelastic component of porosity, and Λ is the thermal pressurization parameter, equal to the ratio of thermal expansivity to compressibility [Rice, 2006]. The second term on the right-hand side is thermal pressurization, the third dilatancy/compaction. Dilatancy acts as a fluid pressure sink, whereas thermal pressurization acts as a pressure source. For spatially uniform permeability, the transport term can be written in terms of the hydraulic

diffusivity $c_{\rm hyd} = \kappa/\eta\beta$. As for the heat equation, the effect of the shear zone thickness can be neglected for times long compared to the characteristic pore fluid diffusion time across the shear zone. Segall et al. [2010] show that, assuming that dilatancy (and compaction) act only normal to the shear zone, $h\dot{\phi} = (1-\phi)\dot{h}$, where $\dot{h}$ is the change in thickness of the shearing layer. In the limit $h \to 0$, and assuming uniform hydraulic properties, the pore pressure diffusion equation reduces to [Segall et al., 2010]

$$\frac{\partial p}{\partial t} = c_{\rm hyd}\frac{\partial^2 p}{\partial y^2} + \Lambda\frac{\partial T}{\partial t}; \qquad \left.\frac{\partial p}{\partial y}\right|_{y=0} = \frac{h\dot{\phi}}{2\beta c_{\rm hyd}}. \tag{4}$$

Laboratory experiments show that the friction coefficient f depends on the instantaneous slip speed v and the past sliding history, which can be characterized by one or more internal state variables θ. We employ the regularized form of the rate-state equations due to Rice et al. [2001], with a single state variable:

$$f(\theta, v) = a \text{ arcsinh}\left[\frac{v}{2v_0}\exp\left(\frac{f_0 + b\ln(\theta v_0/d_c)}{a}\right)\right]. \tag{5}$$

The material constants a and b, which determine the direct velocity and state dependence, respectively, depend on ambient temperature (but are assumed constants here, see [Bizzarri, 2011] for explicit temperature dependence) and hence depth in the earth; v_0 is a normalizing constant; and f_0 is the nominal friction.

The frictional state is sometimes interpreted as the average asperity contact lifetime, and evolves over a characteristic displacement d_c. The proper mathematical description of state evolution has not been resolved (and may not be fully described by any simple analytical representation), although two forms in wide use are the following [Marone, 1998]:

$$\begin{aligned} \frac{d\theta}{dt} &= 1 - \frac{\theta v}{d_c} \\ \frac{d\theta}{dt} &= -\frac{\theta v}{d_c}\ln\left(\frac{\theta v}{d_c}\right). \end{aligned} \tag{6}$$

The first exhibits healing in stationary contact ($v = 0$) and is thus referred to as the "aging" law. In the second form state evolves only with slip ($d\theta/dt$ vanishes when $v = 0$), and is thus referred to as the "slip" law. In both cases the steady-state value of θ is d_c/v. For sufficiently large v, the steady-state friction varies with $(a-b)\ln(v/v_0)$.

Rice and Ruina [1983] showed that slip on the surfaces of two elastic half-spaces pressed together, with effective normal stress $\bar{\sigma}$ and with steady-state velocity weakening friction ($a-b < 0$), is stable/unstable if the dimensions of the slipping zone are less/greater than a critical nucleation dimension

$$h^* \equiv \frac{d_c\mu/(1-\nu)}{(\sigma - p^\infty)(b-a)}\ . \tag{7}$$

Here deformation is plane strain, and μ and ν are the shear modulus and Poisson's ratio.

We use constitutive laws for the inelastic change in porosity $\delta\phi$, including both dilatancy and compaction, that follow Segall and Rice [1995] and are motivated in part by experiments of Marone et al. [1990]. One form associates dilatancy/compaction with changes in the average lifetime of asperity contacts within the fault gouge Segall and Rice [1995]:

$$\delta\phi = -\epsilon\ln\left(\frac{v_0\theta}{d_c}\right) \tag{8}$$

$$\frac{d\phi}{dt} = -\epsilon\frac{d}{dt}\ln\left(\frac{v_0\theta}{d_c}\right) = -\frac{\epsilon}{\theta}\frac{d\theta}{dt}, \tag{9}$$

where $d\phi/dt$ is the rate of inelastic change in pore volume and ϵ is an empirically derived constant of order 10^{-4} Marone et al. [1990]. Above steady state, that is, for $\theta > d_c/v$, θ decreases (from (6)) and the gouge dilates; below steady-state, θ increases and the gouge compacts.

An alternative form posits a velocity-dependent steady-state porosity, but does not directly associate dilatancy with the frictional state variable Segall and Rice [1995]. The porosity, however, seeks steady state with the same distance scale as friction, d_c, consistent with lab observations:

$$\frac{d\phi}{dt} = -\frac{v}{d_c}(\phi - \phi_{ss}) \qquad \phi_{ss} = \phi_0 + \epsilon \ln\left(\frac{v}{v_0}\right). \tag{10}$$

The two forms are actually equivalent for the slip evolution law [Segall and Bradley, 2012]. Experiments on fine quartz gouge confirm that the steady-state porosity increases logarithmically with velocity step [Samuelson et al., 2009] and lead to estimates of $\epsilon \sim 0.5$ to 3×10^{-4}.

3 Results

Segall et al. [2010] analyze the above system of equations under isothermal conditions, to study the effectiveness of dilatancy in producing slow slip events. We defined a non-dimensional dilatancy efficiency as $E_p \equiv \epsilon h/(\beta(\sigma - p^\infty)\sqrt{v^\infty/c_{hyd}d_c})$. Slow slip is favored by strong dilatancy ϵh, low effective stress, compressibility, and diffusivity. The ratio of E_p to thermal pressurization efficiency scales inversely with effective stress showing that high ambient pore-pressures favor slow slip events, consistent with some seismic observations. For $E_p \sim 10^{-3}$ simulated transient slip-rates and repeat times are comparable to that observed in Cascadia. For a broad range of parameters simulations exhibit slow phases driven by down-dip, steady plate motion and faster phases that relax the accumulated stress. The faster phases are assumed to model geodetically observable SSE; the slow phases may help to explain tremor observed between strong SSE.

Segall and Bradley [2012] extend the above calculations to include thermal, as well as pore-pressure, effects. We conduct two-dimensional quasi-dynamic simulations that include rate-state friction, dilatancy, and heat and pore fluid flow normal to the fault. We find that at lower background effective normal stress ($\bar{\sigma}$), slow slip events occur spontaneously, whereas at higher $\bar{\sigma}$, slip is inertially limited. At intermediate $\bar{\sigma}$, dynamic events are followed by quiescent periods, and then long durations of repeating slow slip events. In these cases, accelerating slow events ultimately nucleate dynamic rupture. Zero-width shear zone approximations are adequate for slow slip events, but substantially overestimate the pore pressure and temperature changes during fast slip when dilatancy is included.

In order to better understand slow slip in subduction zones such as Cascadia we developed models of dipping faults in an elastic half-space with depth variable friction and effective stress (Fig. 1). Elastic Green's functions are computed using a boundary element approach, including slip-to-normal stress coupling (which arises due to free surface effects). Slip at a constant rate v^∞ is applied below some depth z_{pl}. To date we have taken the distribution of frictional properties following Liu and Rice [2009]. These authors make use of lab friction experiments on gabbros [He et al., 2007], which show large scatter, but can be interpreted to show a transition from velocity weakening to strengthening behavior at $T \sim 510°$C. This is in contrast to the transition at $\sim 350°$C for granites under fluid saturated conditions. The resulting distribution of $a - b$ mapped to depth using a Cascadia geotherm is shown in Fig. 1.

Early simulations showed that thermal pressurization overwhelms velocity strengthening friction, causing dynamic ruptures to propagate well into the strengthening region. For this

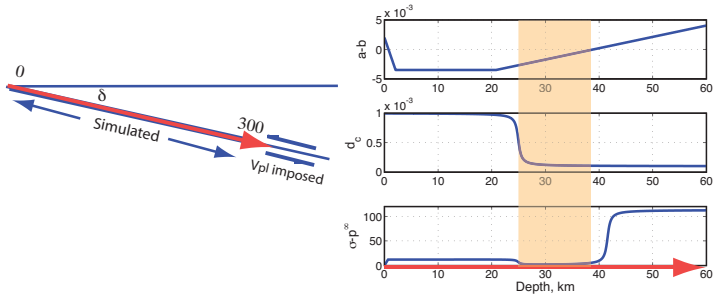

Figure 1: a) Geometry of the dipping fault models. Fault dips at angle δ. Fixed slip rate at v^∞ at the bottom of the model. b) Distribution of $a-b$, d_c, and $\sigma - p^\infty$. $a-b$ distribution from Liu and Rice [2009].

reason, we suppress thermal pressurization at depth where $a > b$. An increase in shear zone thickness at depth would reduce frictional heating. We can more simply simulate this by increasing the heat capacity. For sufficiently high $\bar{\sigma}$ this is effective at stopping dynamic ruptures.

Based on seismic imaging studies and uniform property simulations, we take $\bar{\sigma}$ in the depth range 25 to 40 km to be of order 2 MPa. At seismogenic depths, for results shown here, we take $\bar{\sigma} \sim 12$ MPa, while for $z > 40$ km $\bar{\sigma}$ is ~ 120 MPa. We have found that the latter is required to keep the dynamic ruptures from propagating deep into the velocity strengthening region. Even without thermal pressurization at these depths, the large thermally induced stress drop drives dynamic rupture into regions with $a > b$ but low $\bar{\sigma}$. The low effective-stress velocity-weakening region (shaded in Fig. 1) is where we anticipate SSE to nucleate, and indeed this is the case. Within this region we take $d_c = 100\mu$m, increasing for numerical reasons to 1 mm updip.

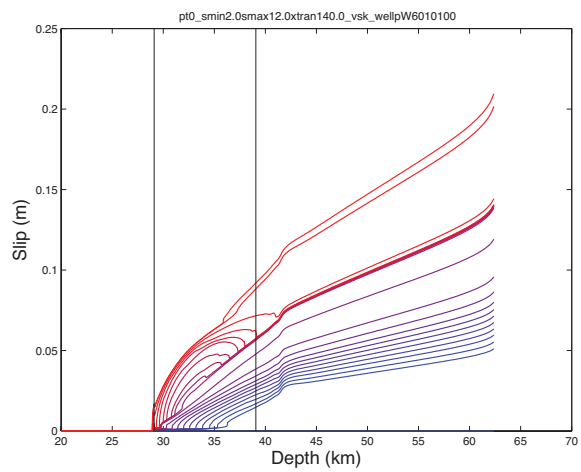

Figure 2: Distribution of slip with depth at different snapshots in time (from early blue to later red) for typical model slow slip event. Vertical lines mark the transition to low effective stress and also to velocity strengthening friction.

A sample result in Fig. 3a illustrates three dynamic events spaced every ~ 200 years. Following dynamic events, the transition between stable sliding and locked fault migrates up-dip for ~ 100 years, (note this transition zone is not fixed as it is in typical kinematic inversions of geodetic data), at which point SSE spontaneously develop. For this distribution of $\bar{\sigma}$, the SSE successively penetrate further updip with time, ultimately nucleating the next dynamic event. The behavior changes somewhat when the width of the low-stress velocity weakening region is reduced to 60 km, such that it is limited to depths of 30 to 40 km (Fig. 3b). Dynamic events, spaced every 300 years, are followed by a stable period and then over 100 years of spontaneously generated SSE. In this case the updip extent of the model SSE is limited by the size of the low $\bar{\sigma}$ region. If this better approximates what occurs in nature, we would not expect to see SSE propagating up-dip with time late in the seismic cycle.

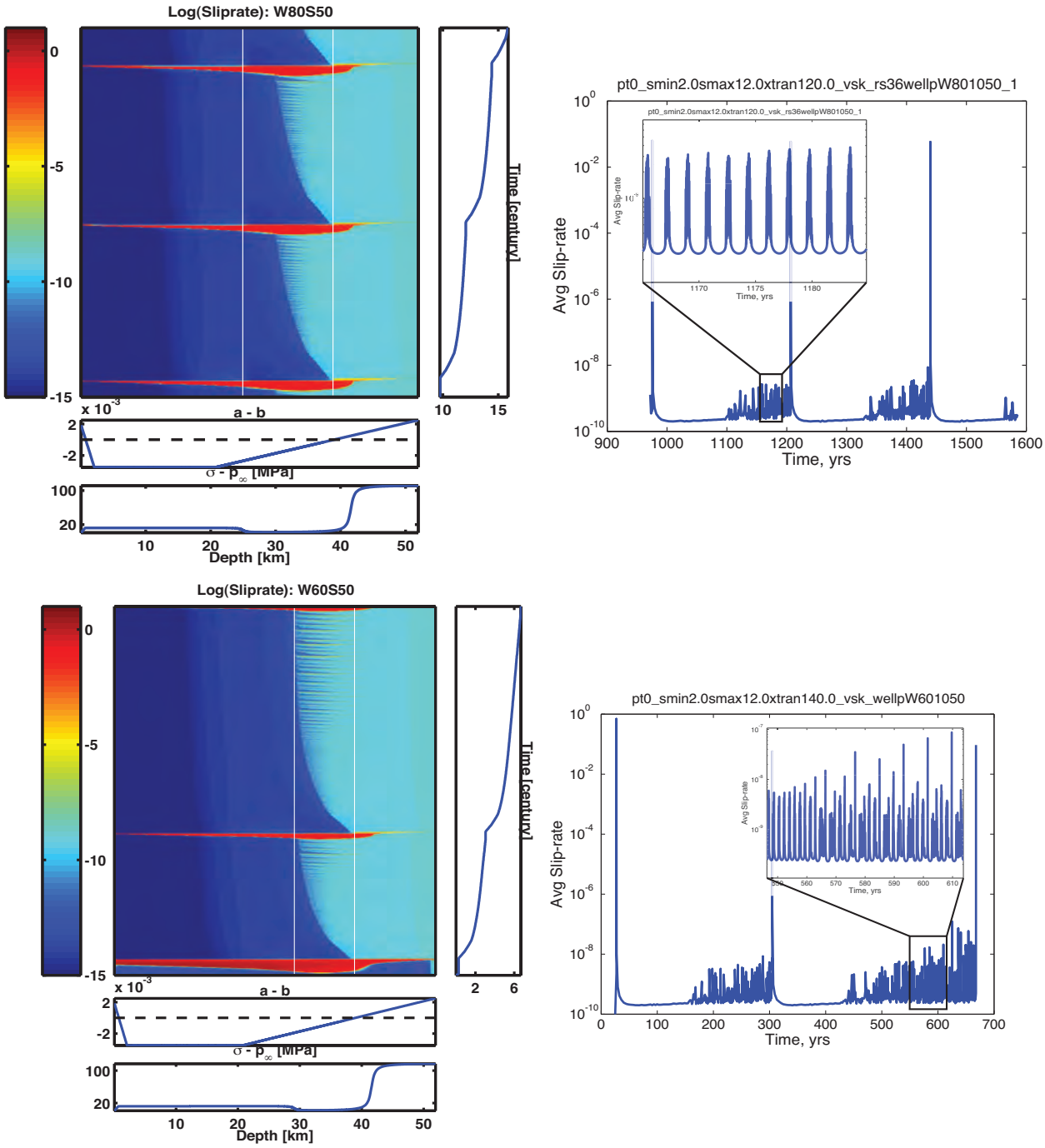

Figure 3: Space-time distribution of slip rate when the low-stress velocity-weakening region is 80 (top) or 60 (bottom) km wide. Time axis is proportional to solver time steps; mapping to physical time is shown in right subpanel. Red streaks are dynamic slip events; light to dark blue streaks are slow-slip events. Right) Spatially averaged slip speed with time, showing dynamic events and regularly spaced SSE (insert).

Fig. 2 illustrates slip during a model SSE (parameters similar to Fig. 3b but with broader strengthening region). Similar to the results with uniform properties, there is a slow phase that propagates up-dip over roughly one year, followed by a more rapid (but quasi-static) transient slip event. Note that the transient event is localized to $\sim 29 < z < 42$ km. As in the uniform property simulations, the fault is never quiescent; there is always some propagating slip occurring. It is tempting to associate the slower phase (in blue in Fig. 2) with inter-ETS tremor and deformation observed by borehole strainmeters [Roeloffs and McCausland, 2010].

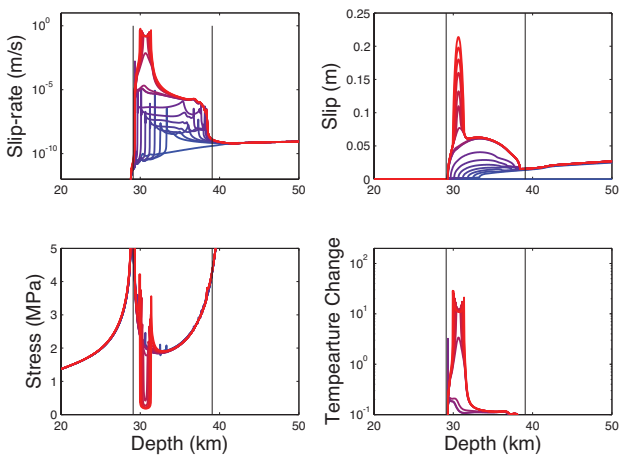

Figure 4: Nucleation of dynamic event. a) slip rate b) slip c) shear stress d) temperature change. Curves are snapshots in time from early (blue) to late (red). Vertical lines mark the low $\bar{\sigma}$, velocity weakening region.

As the model SSE continue, the maximum slip speed during an event generally increases. Ultimately slip rates reach a level where thermal pressurization becomes important and the fault accelerates to dynamic instability. Fig. 4 shows a SSE accelerating to $\sim 10^{-5}$ m/s, at which point T begins to increase by a few degrees. This is sufficient to increase the stress drop, leading to nucleation of dynamic slip. The dynamic event propagates up-dip to the free surface as well as down-dip, intruding somewhat into the velocity strengthening region (Figure 3). Note that, in part because the SSE do not accommodate the full plate motion, dynamic slip propagates through the ETS zone. If this accurately describes Cascadia, it has important implications for seismic hazards there.

It is widely recognized that ETS events shed stress to the locked megathrust. Some discussion has been given to whether or not stress variations due to ETS leads to time varying probability of triggered earthquakes using Dieterich's [1994] seismicity-rate theory. Another possibility, observed in our simulations, is that SSE grow into dynamic ruptures. Understanding which of these might occur and how to distinguish between them has obvious implications for assessing time dependent seismic hazard.

When the size of the low-$\bar{\sigma}$ velocity weakening region is large, as in Fig. 3, model SSE steadily penetrate further updip, with generally increasing maximum slip speed. Ultimately slip rates reach a threshold where thermal pressurization becomes important and the fault accelerates to dynamic instability. Fig. 4 shows a SSE accelerating to $\sim 10^{-5}$ m/s, at which point T begins to increase by a few degrees. This is sufficient to increase the stress drop, leading to nucleation of dynamic slip. The dynamic event propagates to the free surface as well as down-dip, intruding somewhat into the velocity strengthening region (Figure 3). In contrast, when the low-$\bar{\sigma}$ velocity weakening region is relatively smaller, as in Fig. 3(bottom), the model SSE become trapped in this region. This results in a strong stress concentration immediately above the ETS zone, which ultimately leads to the nucleation of a dynamic event at the up-dip boundary of the ETS zone.

4 Relationship between tremor and slow slip

One hypothesis for occurrence of tremor is that locally locked asperities within the SSE region are loaded by the surrounding slip, leading to localized dynamic rupture. This suggests that tremor is favored in areas of high slip-rate immediately behind the slow slip front. To test this we inverted daily GPS positions for the space-time evolution of slip and slip-rate on the plate interface during the August 2009 ETS event, and compared the slip-rate to tremor hypocenters independently located by the Univ. of Washington group, using waveform envelope correlation. We analyzed daily GPS positions from 101 PBO stations, roughly 40 of which show measurable signal during the ETS event. Secular and seasonal signals are fit and removed prior to inversion. Following this, we estimate slip and slip-rate as a function of position and time with a Network Inversion Filter [Segall and Matthews, 1997], along with local benchmark motion and daily corrections to the GPS reference frame, modified for non-negative slip-rate. Spatial and temporal smoothing was estimated by a combination of maximum likelihood and inspection of time-series fits.

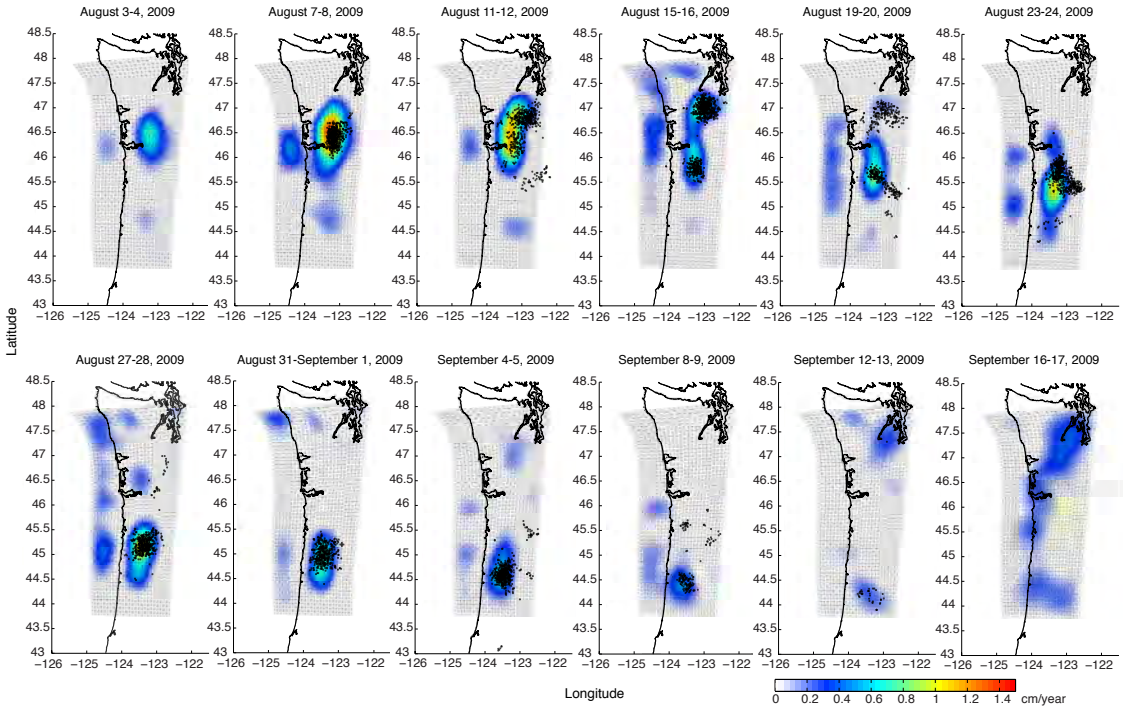

Figure 5: Slip rate on the plate interface, averaged over two day intervals during the August 2009 SSE in Cascadia. Tremor hypocenters are plotted in black for the same two-day intervals. Each hypocenter represents the best fit location of tremor for a 5 minute window in which tremor is detected. The plate interface mesh is shown between 10 and 60 km depth. From Bartlow et al. [2011].

Snapshots of slip-rate and tremor averaged over two day intervals are shown in Figure 5. Tremor starts near 46.5° N on August 6 and propagates both north and south. Slip is observed in the first panel of Fig. 5, prior to the tremor onset. This premature slip results from a well known artifact of temporal smoothing, and is absent in non "back-smoothed" results [Bartlow et al., 2011]. By August 15 tremor has split into two groups; the northern cloud disappears soon after, while the southern cloud continues to propagate south. Inversion of the GPS data

resolves a similar splitting and migration of the slipping region (Figure 5). In sum, we find an excellent correlation between the instantaneous region of high slip rate and tremor hypocenters for all times during the ETS event (Figure 5). This correlation is especially remarkable given that tremor hypocenters and slip are obtained from completely independent data. To test the resolution of the inversion we construct synthetic data from an elliptical slip distribution which propagates north-south at a constant rate. These tests show that the inversion correctly locates the position of maximum slip-rate behind the SSE slip-front.

5 Bibliography supported by this grant, exclusive of abstracts

1. P. Segall, A. Rubin, A. M. Bradley, and J.R. Rice. Dilatant strengthening as a mechanism for slow slip events. *Jour. Geophys. Res.*, 115:37, 2010. 10.1029/2010JB007449.

2. Noel M. Bartlow, Shin'ichi Miyazaki, Andrew M. Bradley, and Paul Segall. Space-time correlation of slip and tremor during the 2009 cascadia slow slip event. *Geophys. Res. Lett.*, 38(18):L18309–, September 2011. ISSN 0094-8276.

3. P. Segall and A. M. Bradley. Slow vs fast slip due to competition between thermal pressurization and dilatant strengthening. *Journal of Applied Mechanics-Transactions of the ASSME*, in press, 2012.

References

Noel M. Bartlow, Shin'ichi Miyazaki, Andrew M. Bradley, and Paul Segall. Space-time correlation of slip and tremor during the 2009 cascadia slow slip event. *Geophys. Res. Lett.*, 38(18):L18309–, September 2011. ISSN 0094-8276. URL `http://dx.doi.org/10.1029/2011GL048714`.

A. Bizzarri. Temperature variations of constitutive parameters can significantly affect the fault dynamics. *Earth and Planetary Science Letters* ., 306, doi:10.1016/j.epsl.2011.04.009:272–278, 2011.

C. He, Z. Wang, and W. Yao. Frictional sliding of gabbro gouge under hydrothermal conditions,. *Tectonophysics*, 445:353– 362, 2007.

A. H. Lachenbruch. Frictional heating, fluid pressure, and the resistance to fault motion. *Journal of Geophysical Research*, 85:6097–6112, 1980.

N. Lapusta and Y. Liu. Three-dimensional boundary integral modeling of spontaneous earthquake sequences and aseismic slip. *Journal of Geophysical Research*, 114:B09303, 2009. doi: 10.1029/2008JB005934.

Y-J Liu and J. R. Rice. Slow slip predictions based on granite and gabbro friction data compared to GPS measurements in northern Cascadia. *Journal Geophysical Research*, 114, 2009. doi: 10.1029/2008JB006142.

Y. J. Liu and A. Rubin. Role of fault gouge dilatancy on aseismic deformation transients. *Journal of Geophysical Research*, 115:B10414, 2010. doi: 10.1029/2010JB007522.

C. Marone. Laboratory-derived friction laws and their application to seismic faulting. *Ann. Rev. Earth Planet. Sci*, 26:643–696, 1998.

C. Marone, C.B. Raleigh, and C.H. Scholz. Frictional behavior and constitutive modeling of simulated fault gouge. *Journal of Geophysical Research*, 95:7007–7025, 1990.

J. R. Rice, N. Lapusta, and K. Ranjith. Rate and state dependent friction and the stability of sliding between elastically deformable solids. *Journal of Mechanical and Physical Solids*, 49: 1865–1898, 2001.

James R. Rice. Heating and weakening of faults during earthquake slip. *J. Geophys. Res.*, 111: B05311, 2006. doi: 10.1029/2005JB004006.

J.R. Rice. Spatio-temporal complexity of slip on a fault. *Journal of Geophysical Research*, 98: 9885–9907, 1993.

JR Rice and AL Ruina. Staibility of steady frictional slipping. *Journal of Applied Mechanics-Transactions of the ASSME*, 50(2):343–349, 1983. ISSN 0021-8936.

J. Samuelson, D. Elsworth, and C. Marone. Shear-induced dilatancy of fluid-saturated faults: Experiment and theory. *Journal of Geophysical Research*, 114:B12404, 2009. doi: 10.1029/2008JB006273.

P. Segall and A. M. Bradley. Slow vs fast slip due to competition between thermal pressurization and dilatant strengthening. *Journal of Applied Mechanics-Transactions of the ASSME*, in press, 2012.

P. Segall, A. Rubin, A. M. Bradley, and J.R. Rice. Dilatant strengthening as a mechanism for slow slip events. *Jour. Geophys. Res.*, 115:37, 2010. doi: 10.1029/2010JB007449.

Paul Segall and James R. Rice. Dilatancy, compaction, and slip instability of a fluid-infiltrated fault. *J. Geophys. Res.*, 100(B11):22155–22171, 1995.

T. Suzuki and T. Yamashita. Dynamic modeling of slow earthquakes based on thermoporoelastic effects and inelastic generation of pores. *Journal of Geophysical Research*, 114:B00A04, 2009. doi: 10.1029/2008JB006042.

T Yamashita and T Suzuki. Dynamic modeling of slow slip coupled with tremor. *Jour. Geophys. Res.*, 116 B05301:doi:10.1029/2010JB008136, 2011.